Polymer 49 (2008) 3841–3854

Contents lists available at ScienceDirect

Polymer

journal homepage: www.elsevier.com/locate/polymer

Feature Article

Polymers with aligned carb

S.V. Ahir, Y.Y. Huang, E.M. Terentjev*

Cavendish Laboratory, University of Cambridge, J.J. Thomson Avenue, Cambridge CB3 0HE, UK

ARTICLE INFO

Article history:
Received 1 April 2008
Received in revised form 3 May 2008
Accepted 7 May 2008
Available online 10 May 2008

Keywords:
Carbon nanotubes
Composites
Actuation

ABSTRACT

We review the current state of the polymer–carbon nanotube composites field. The article first covers key points in dispersion and stabilization of nanotubes in a polymer matrix, with particular attention paid to ultrasonic cavitation and shear mixing. We then focus on the emerging trends in nanocomposite actuators, in particular, photo-stimulated mechanical response. The magnitude and even the direction of this actuation critically depend on the degree of tube alignment in the matrix; in this context, we discuss the affine model predicting the upper bound of orientational order of nanotubes, induced by an imposed strain. We review how photo-actuation in nanocomposites depend on nanotube concentration, alignment and entanglement, and examine possible mechanisms that could lead to this effect. Finally, we discuss properties of pure carbon nanotube networks, in form of mats or fibers. These systems have no polymer matrix, yet demonstrate pronounced viscoelasticity and also the same photomechanical actuation as seen in polymer-based composites.

1. Introduction

This review is devoted to nanotube–polymer composite materials. Some fundamental studies of mesh networks made purely of nanotubes are presented towards the end to highlight parallels and contrasts with an ordinary polymer network. Aspects of nanotube dispersion and alignment in the matrix are also discussed, with particular attention given to limitations of traditional surface techniques to characterize nanotube–polymer composites. The main focus, however, belongs to the photomechanical actuation of nanotube–polymer composites. Here we review the phenomenon, its amplitude and dynamics, and discuss possible mechanisms that can explain how the absorption of light leads to the mechanical response of nanocomposites. Photo-actuation of nanotube–polymer systems demonstrates an exciting example of what is possible above and beyond improvements in existing carbon fiber technologies.

Composites as a class of materials have existed for millennia and are prevalent both in nature and among engineering materials. A definition of a classical composite is a continuous system with inhomogeneities of a size much greater than the atomic length scale (allowing us to use classical physics), but is essentially homogeneous macroscopically. A number of substantial monographs illuminate this field of study, e.g. [1,2].

The practice of creating synthetic polymer-based composites originates from pioneering work in the 1970s on carbon fiber reinforced thermosets and thermoplastics, with many reviews and books in the field [3–6]. There has always been an interest in carbon in its fibrous form due to its covalent in-plane bonding, considered amongst the strongest in nature, imparting a great deal of structural strength. It is essentially the same bonding regime as found in individual graphene sheets within graphite. Accordingly, carbon fiber is an ideal reinforcing agent.

But what would make a better fiber? Issues of processability and cost of production aside, the perfect fiber would have to be free of defects and possess a structure akin to single-crystal graphite. Carbon fibers currently in use contain large amounts of structural defects and impurities along the surface which often disable their ability to achieve strength, toughness and conductivities approaching their theoretical limit. An ideal nanometer-sized fiber would also raise the possibility of having a quasi-one-dimensional structure embedded in the continuous elastic matrix, which would be of immense benefit to fundamental scientific research, for example, testing a multitude of physical phenomena that are dimensionally correlated [7].

The most celebrated of these nanometer-thick structures is a tube made of carbon with an acicular single-crystal structure much like a tubular version of fullerene, termed carbon nanotubes. The seminal paper by Iijima [8] is widely regarded as having introduced and started the nanotube revolution. However, the first patent regarding nanotubes was registered as early as 1987 by Hyperion [9], the first images of a nanotube were produced back in 1975 [10] though at the time, it was not given any thought or focus. Clearly, nanotubes were seen before 1991 but it was only after Iijima's work that global scientific attention was rightly turned to this fourth allotrope of carbon. Multi-wall carbon nanotubes

* Corresponding author.
E-mail address: emt1000@cam.ac.uk (E.M. Terentjev).

0032-3861
doi:10.1016/j.polymer.2008.05.005

(MWCNT) were first reported in 1991 [8], and the single-wall variety (SWCNT) followed soon after [11–13].

The actual arena of nanotube–polymer composites was first introduced by Ajayan [14]. Though that work was initially directed towards aligning the tubes in any given medium, it proved an important milestone demonstrating the proof of concept and, together with other early work [15–18], showed that the remarkable properties indigenous to the tubes could be transferred to the polymer matrix. Another interesting avenue of research involves manipulation of the tube chemistry, which also presents the opportunity to develop multifunctional composites with tailored physical properties. By the end of 2003, 59 out of 152 nanotube patents existed in relation to nanotube composites, their processability and production [19]. Since the early work from 1990s, an explosion of literature and scientific debate has surfaced. Much has been garnered from nanotechnology research, with over 10 papers a week currently appearing in relation to nanotube–polymer composites alone.

Once the nanotubes have been processed and purified to an acceptable level, the next stage in production of a composite is to homogeneously disperse the tubes into the polymer matrix. There are many benefits of completing such a procedure thoroughly. Primarily, one needs to ensure that the properties of the composite are homogeneous throughout. Additionally and perhaps more appropriate to nanotubes, a homogeneously dispersed filler in the polymer matrix reduces the possibility of nanotube entanglement, which can lead to significant changes in composite behavior [20–22]. The nanotube aggregation within a polymer system would certainly have a negative impact on its stiffening ability [23]. As yet, the nature of these entanglements and their influence on the composite properties is a little understood area.

As is well known from the Onsager treatment of anisotropic suspensions [24], the overlap concentration, when highly anisotropic particles start interacting and significantly biasing their pair correlation, is inversely proportional to the aspect ratio – and so can be very low indeed for nanotubes which typically have very high aspect ratios. Additionally, the nanotubes must *remain* in this uniformly dispersed state, and not re-aggregate in spite of the inevitable van der Waals attractive interaction between them. The other problem is to monitor the quality of dispersion, that is, the size of the remaining aggregates in the bulk. This is an important and delicate point. Early reports in the literature often claimed that homogeneous dispersions had been achieved, when in truth only dispersions of aggregates of tubes had been established, but hard to detect in the bulk of a composite when they are smaller than 2–300 nm.

Dispersion involves separation and then stabilization of CNTs in a medium. For best decision on the choice of technique for a particular system, it is essential to distinguish and study these two processes individually, which we shall discuss in the next section in some detail. The remainder of this review is focused on the new and remarkable effect exhibited by the nanotube–polymer composites: the photo-induced mechanical actuation. Actuation in soft materials is much sought after due to possible links with artificial muscles [25]. Non-contact photo-induced actuation is especially relevant, and opens access to engineering of micro-optomechanical systems (MOMS) [26]. The special feature of actuation process in carbon nanotube composites is the equilibrium (fully reversible) nature of the effect [27], which is a great advantage over most shape-memory systems that only have a one-way actuation. The final chapter of this review describes the pure nanotube network, which is not nominally a composite, but is also shown to demonstrate a similar photo-actuation and is very useful to compare with the polymer-based composites.

2. Dispersion of CNTs in polymers

Dispersion and stabilization of particles in a continuous (most often – fluid) matrix is a classical problem in colloid science. It has been recognized for a century that in order to overcome the primary potential well of van der Waals (VDW) attraction one needs to use surface-active compounds. Surfactants, whose physico-chemical nature may vary greatly, help to reduce the attraction and/or prevent particles from coming close enough to proximity to get trapped in this potential well. After addition of the appropriate stabilizing agent, it is just a question of shear stress to disperse the particles in the matrix.

With carbon nanotubes, two new factors come into consideration: in many situations the subsequent applications require the neat, highly electronically active surface of CNTs to be preserved (i.e. not covered by a surfactant), and also – the extremely high aspect ratio makes CNTs vulnerable to breaking under shear exceeding a certain threshold. Effective separation requires the overcoming of the inter-tube VDW attraction, which is anomalously strong in CNT case due to their high polarizability. Depending on the tube shape/sizes and the orientation of tubes with respect to each other, such an attraction can act within a spacing of a few nanometers [28]. For closely packed tubes, the surface adsorption of dispersant or the wetting of the polymer/solvents requires an initial formation of a temporary (partial) exfoliation state [29]. Mechanical stirring/mixing, and increasingly commonly ultrasonication, are employed for this purpose, both providing the local shear stress which breaks down the bundles.

In the end, the dispersion of nanotubes in polymer matrix is a matter of experimenting. The large variation of tubes exists (differing in synthesis process, impurities, surface chemistry, etc.), and the different application requirements mean that the suitability of a dispersion technique is system-dependent. A vast amount of literature is available on nanotube dispersion in aqueous and organic solutions, with or without the aid of extensive surface functionalization, with some good reviews available [30,31]. Here we would like to focus only on the dispersion techniques which can optimally preserve the intrinsic electronic and mechanical properties of an isolated CNT.

As-produced CNTs are present in a wide range of morphologies. Single-wall tubes tend to orient parallel to each other in close proximity to maximize their interaction, thus forming bundles consisting of 100–500 tubes (0.2–1 μm bundle diameter) [32]. Girifalco developed a model to calculate the effective VDW interaction between infinitely long SWNTs [28]. By assuming that the tube–tube interactions are negligible at distances over twice the diameter, the cohesion energy of a 1 nm diameter tube in a bundle is calculated to be −0.36 eV/Å, with equilibrium spacing between tubes of ~25 Å. The validity of this model for MWCNTs is not clear, however, a classical solution is available which describes the VDW interaction energy between two mesoscopic cylinders of length L, diameter d, separated by a gap H, in parallel and perpendicular contact configurations:

$$V_{\parallel} \sim -\frac{A}{24} L d^{1/2} H^{-3/2} \quad \text{and} \quad V_{\perp} \sim -\frac{A}{6}\frac{d}{H}, \quad \text{for} \quad H < d, \qquad (1)$$

where A is the Hamaker constant which depends on polarizability of the particles and the surrounding matrix, $A \sim 2 \times 10^{-19}$ J [33] for CNTs in a medium with permittivity $\varepsilon \geq 1$. Therefore, for two identical tubes of diameter $d = 10$ nm and contour length $L = 10$ μm, aligned parallel to each other with a separation $H = 1$ nm, the VDW interaction is $\sim 2 \times 10^{-16}$ J per tube; for crossing configuration, this energy is $\sim 3 \times 10^{-19}$ J ($\sim 100 k_B T$) per contact. Separation of tubes from a bundle requires the shear energy delivered to the bundle to exceed the characteristic values associated with these two different configurations.

2.1. Ultrasonication

Ultrasonication is widely employed in CNT dispersion, where separation and functionalization of the tubes can be greatly enhanced. The two main instruments used are ultrasonic bath (40–50 kHz), and ultrasonic horn/tip (25 kHz) [31]. The conditions which controls chemical and mechanical effects of sonication include [34,35]: the ultrasound intensity and frequency; the pulsing interval and duration; the presence of gases; the external pressure and temperature; the location of the ultrasound source and the container geometry; and the concentration of solute. At the same time, one often finds the dependence on solvent viscosity and surface tension to be weak. All of the above factors determine the formation and nature of ultrasonic cavitation. Upon bubble implosion, temperatures and pressures of up to 15 000 K and 1000 atm can be created [35,36]. Free radicals are subsequently produced in the molecules exposed to these temperatures and the oscillating high pressure induces shock waves in the liquid. It is this process which enhances the chemical reactivity in the solution, and also gives rise to erosion and breakage of the solutes [37]. In the following analysis, effects of ultrasonication on the integrity of CNTs are discussed.

The first question one needs to address is the level of shear forces that can be attained in a common sonication process. In the first instance, let us assume a simple rectangular ultrasonic bath geometry, where a stationary pressure gradient is established with no cavitation. For a typical ultrasonic power output of 100 W and frequency 25 kHz, the corresponding wavelength of sound in a typical liquid (e.g. water) is $\lambda \sim 5$ cm. The corresponding peak pressure in the wave is of the order $\Delta P \sim 1$ atm $= 10^5$ Pa, giving the stress applied to the tube of length L of the order $\Delta P(L/\lambda) \sim 20$ Pa. Clearly this is not sufficient to separate tubes from the bundles, let alone induce tube breakage.

As the power density exceeded certain critical values [34], cavitation takes place. Theoretical calculation suggested a fluid strain rate of up to $10^7\ s^{-1}$ outside the bubble during implosion [38], far greater than $\sim 4000\ s^{-1}$ maximum strain rate reported for the shear mixing devices [39]. Clearly, ultrasonication in the cavitation regime is capable to overcome the VDW interactions in various CNT systems. It should be noted that although the separation happens on very short time scales during the bubble implosion (microseconds [40]), the time for the dispersant to diffuse into the opened gap between the tube and the bundle is comparable. For instance, for a typical diffusion coefficient $D \sim 10^{-7}\ m^2/s$ and the (overestimated) distance to diffuse ~ 100 nm, the time this takes is of the order 10^{-7} s. A succession of cavitation events may be required to maintain this separation state for dispersant/solution to penetrate between the tubes.

Alongside with separation, unwanted tube cutting and lattice amorphization often takes place, attributed to the violent cavitation. Multi-walled tubes can get shorter and thinner, going through a layer by layer un-wrapping process [31,41]; SWNTs are also reported significantly shortened, with "dented" openings created on the sidewall [42]. Therefore, sonication is prone to disrupt the integrity, electronic structure and oxidation resistance of CNTs. In addition, one has also to be aware of the much enhanced chemical activity introduced by the high temperature and pressure near imploding bubbles. Solvent polymerization and reactions between solvent and CNTs have been observed [29,43].

How can one avoid tube damage and cutting when applying ultrasonication? In order to answer this question, we first need to determine whether the scission is dominated by thermal or mechanical effects of cavitation (assuming chemically inert environment). The spontaneous and localized temperature in the vicinity (~ 200 nm) of bubble implosion exceeds thousands of Kelvin [35], approaching the melting and vaporization temperatures of graphite ($T_m \approx 4400$ K, $T_v \approx 4700$ K). Therefore, thermal excitation is capable to locally melt the graphite layers. Nevertheless, prevailing evidence is for the dominance of mechanical scission. The key observation is that in various experiments on sonication of CNTs (both MW and SW) the resulting tube length tends to a fixed saturation value L_{lim} after prolonged sonication (the exact value depends on conditions) [44,45]. Hilding et al. [31] observed a scission rate which had a cubic dependence on the MWCNT length. If the process was temperature-controlled, one would expect random scission process with the amount of cut tubes increasing with time.

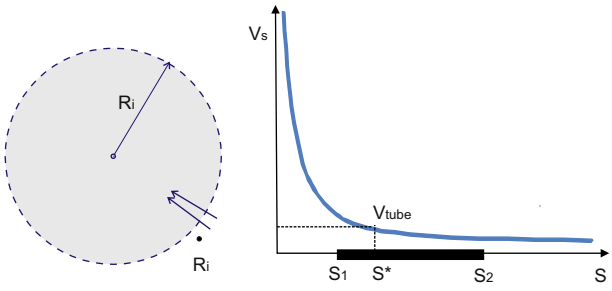

Fig. 1. A snapshot during the cavitation process, showing a bubble of radius R_i collapsing with its wall velocity $\dot{R}_i$. The instantaneous velocity field of the fluid medium surrounding the bubble, V_S, is also illustrated.

To investigate mechanical scission in ultrasonic cavitation, a simplified bubble dynamic concept can be employed, which looks at the radial solvent flow around a single imploding bubble, Fig. 1, and an affine estimate to calculate the force/stress exerted on the nanotube by viscous forces in this region.

Consider the bubble with an instantaneous radius of R_i and wall velocity $\dot{R}_i$. Assume that the tube is in an instantaneous equilibrium and moving with a speed of V_{tube}, such that the total shear forces applied on the tube surface add to zero. The radial fluid velocity at a distance S from the bubble is estimated by $V_S = R_i^2\dot{R}_i/S^2$. There is a point along the tube, at a distance S^*, at which the surrounding fluid moves at the same speed V_{tube}. The local shear stress on the tube surface is estimated by $\eta(V_S - V_{tube})/d$, with d the tube diameter and η the solvent viscosity. Balancing of tensile forces on both sides of S^* gives, after cancelation of factors on both sides:

$$\int_{S_1}^{S^*} (V_S - V_{tube})\mathrm{d}S = \int_{S^*}^{S_2} (V_{tube} - V_S)\mathrm{d}S. \tag{2}$$

Solving this equation gives $S^* = \sqrt{S_1 S_2} = \sqrt{S_1(S_1 + L)}$, which is the location of maximum tensile stress on the tube. Using this value we can re-calculate the integral in Eq. (2) to determine the total force pulling in each direction; dividing this by the tube cross-section area gives the tensile stress exerted on the tube, reaching the maximum at S^*:

$$\sigma_t = \frac{8\eta}{d^2} R_i^2 \dot{R}_i \left[\frac{1}{\sqrt{S_1}} - \frac{1}{\sqrt{S_1 + L}}\right]^2. \tag{3}$$

Taking the typical literature values for the bubble size and rate of implosion ($R_i \sim 10\ \mu$m and $\dot{R}_i/R_i \sim 10^7\ s^{-1}$), the CNT diameter $d \sim 10$ nm, the viscosity of a typical low-molecular weight solvent $\eta \sim 10^{-2}$ Pa s, and $S_1 \sim L \sim 10\ \mu$m, we obtain the estimate for the maximum tensile stress generated by viscous forces near the imploding bubble: $\sigma_t \sim 70$ GPa. This is enough to break most nanotubes! However, it is also clear from Eq. (3) that the tensile stress on the tube decreases dramatically as the tube length L diminishes, and a characteristic threshold length L_{lim} exists for tube scission (for a set of pre-defined parameters η, d and $R_i(t)$). If the

value of breaking stress (ultimate tensile strength) of the nanotube is σ^*, then this threshold length is

$$L_{\lim} = \sqrt{\frac{d^2\sigma^*}{2\eta(\dot{R}_i/R_i)}}. \quad (4)$$

Tubes shorter than $L_{\lim}$ will not experience scission anymore!

The suitability of the above affine flow model to describe the breakage of individual SWCNTs is not clear due to the smaller persistence length, and higher flexibility of tubes compared to MWCNTs [46]. Another apparent deficiency of the above model is that the instant shear force is linearly dependent on viscosity, while the experiment suggests only a weak dependence of scission on viscosity during sonication. This is probably because of the offsetting effect of increasing ultrasound absorption and a much lower probability of cavitation at higher viscosities. Strictly, Eqs. (3) and (4) are only applicable to low-viscosity solvents. Nevertheless, this analysis gives a qualitative picture of the role played by the imploding bubble parameters R_i and $\dot{R}_i$ in tube breakage. In other words, it is possible to establish a shear condition with minimal cavitation and tube scission. The ideal conditions are such that the shear rate is just high enough, and duration is long enough for dispersant/solvent to diffuse into the bundle gap [47]. There are many discrepancies in the literature on sonication conditions due to the mis-reporting of actual power density delivered in different systems. A rough and quick way to evaluate (in a low-viscosity medium) is to measure the average power density delivered to the solution by calorimetry. The generally accepted criteria are 10 W/cm^2 for transient bubble formation [48], and 1–3 W/cm^2 for stable bubble formation. Stable bubbles exist for many cycles and collapse less violently; thus the probability of tube scission is reduced. Other possible areas to explore are such as using ultra-high frequency sonication (i.e. >100 kHz, to limit the growth of bubbles/caviation), or by adding catalytic particles to anneal the defects formed in-situ [49]. Post-sonication high temperature annealing (e.g. at 2000 °C) can also help to restore the crystallinity of the CNTs to some extent [42,50]. In short, in order to obtain reproducible results, it is important to keep the experiment setup highly consistent.

2.2. Shear mixing

Mechanical separation of CNTs from bundles can also be achieved in shear flow induced by stirring, rotation of extrusion of a polymer solution or melt. Usually, direct separation by shear mixing is only achievable for specific types of MWCNTs, with high shear rates in a rather viscous medium. However, the parameters of shear mixing are more controllable, and better integrity of dispersed CNTs can be obtained compared to ultrasonication. To separate a bundle, the energy delivered to it has to exceed the characteristic values associated with the different tube configurations, see Eq. (1). We will now follow this logic to discuss the effectiveness of shear mixing techniques.

An example of detailed mechanical dispersion study describes MWCNTs prepared by the method of catalytic vapor deposition (CVD), which are initially found in a lightly entangled mesh (without substantial parallel alignment) [51], Fig. 2(a). Tube length was in the range $L \sim 5$–15 μm and the outer diameter $d \sim 60$–100 nm. Given these parameters, and the tube persistence length l_p, one can estimate the characteristic overlap concentration in an ideally dispersed composite. Overlap concentration theoretically marks the boundary between dilute (individual tubes in solution) and semidilute (interpenetrating, entangled tubes) regimes. The overlap volume fraction was estimated as $\phi_c = d^{7/5}l_p^{-3/5}L^{-4/5}$ [51] and for the given MWCNT parameters gives the volume fraction $\phi_c \sim 0.003$–0.008. To make comparisons with experiments (in which one measures the CNT loading by the weight percent), one needs to convert the volume fraction ϕ into the weight fraction. Using the density of nanotubes, $\rho_{tube} \sim 2$ g/cm^3, we estimate the overlap to occur at $n_c \sim 0.5$–1.5 wt%. Above this concentration, the semidilute solution of self-avoiding CNTs will become increasingly entangled and develops the elastic modulus.

Consider a Couette shear mixing geometry with the cell radius $R \approx 7$ mm and gap $h \approx 1.5$ mm filled with the nanotube–polymer mixture, Fig. 2(b). The shear stress can be estimated as $\sigma \sim \eta R\omega/h$, where $\omega \approx 100$ rad s^{-1} is the angular frequency of mixer rotation at 1000 rpm. The viscosity η of the matrix depends on the molecular weight, and was ~5.6 Pa s at 25 °C in PDMS [51]. The resulting estimate of shear stress is of the order of 3 kPa. Using Eq. (1), the VDW energy per inter-tube contact for tubes with $d = 80$ nm is $\sim 10^{-18}$ J. This gives the characteristic shear volume per VDW contact $\sim 3 \times 10^{-22}$ m^3, corresponding to the length scale ~70 nm. In other words, the shear energy supplied by the mixer would be able to separate the tubes if they were on average, spaced more than ~70 nm between contacts. From the SEM image of CNT samples, Fig. 2(a), it is evident that the tubes exposed on the outer surface of the aggregate satisfy this criterion. When being mixed in viscous polymer matrix, the separation process proceeds in analogy to peeling of tube layers from aggregates. This peeling model implies that a certain critical time t^* is needed for all the tubes to be parted, leading to a homogeneous dispersion. At the same time it appears clear that parallel CNT bundles, in which the VDW attraction is active along the whole length of parallel tubes, will be impossible to break down by shear flow that is unlikely to generate local stress above several tens of kiloPascals.

Monitoring the quality of nanotube dispersion in a continuous polymer matrix is a perennial problem, with very few experimental

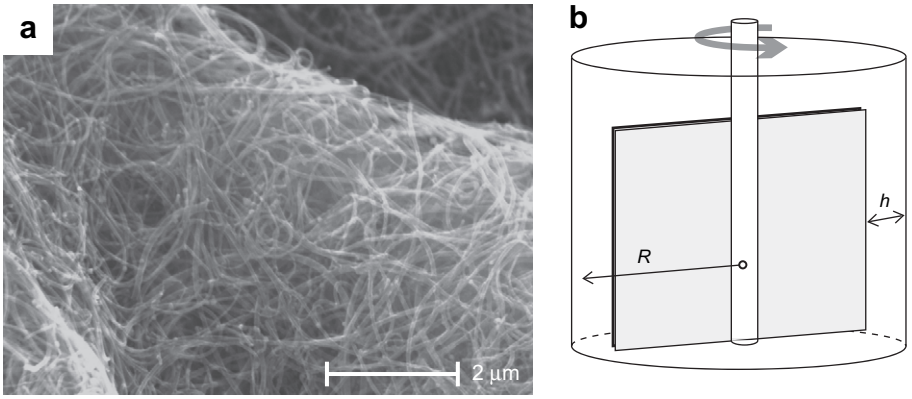

Fig. 2. (a) A typical scanning electron microscopy (SEM) image of nanotube agglomerates, showing the entangled nature of raw samples prepared by the CVD method; (b) scheme of a shear mixing container, with the relevant dimensions labelled for calculation of shear stress.

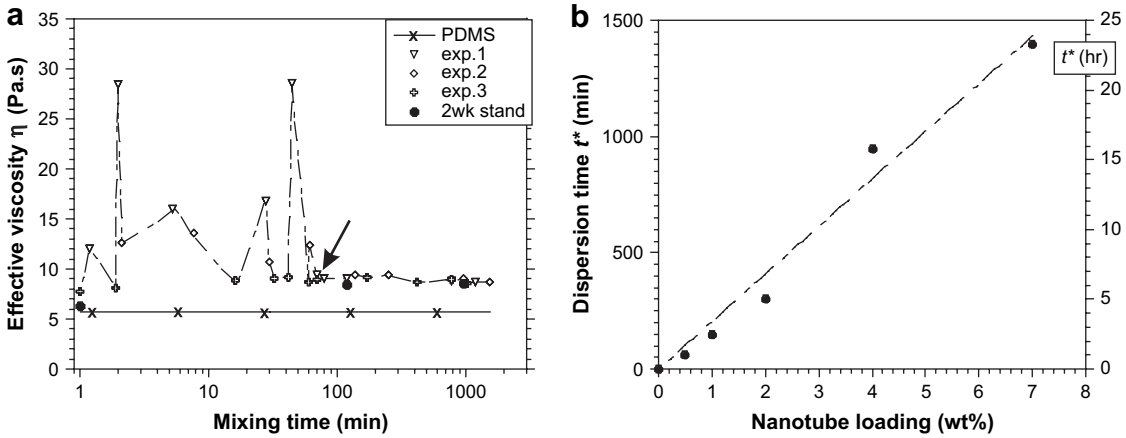

Fig. 3. (a) Effective viscosity, η at 50 Hz, against the time of mixing, for three separate experiments on shear mixing the $n = 1$ wt% CNT sample in PDMS. The arrow marks the characteristic time t^*; (b) dispersion time t^* against the concentration of nanotubes. The right axis shows the same time in hours. The dashed line is the linear fit [51].

techniques available to resolve it. Electron microscopy, which is the only method offering real-space resolution on the scale of nanotubes, is an inherently surface technique. Attempting to dissolve or ion-etch the polymer to reveal the tubes, immediately leads to their re-aggregation. Making samples very thin to allow transmission microscopy makes nanotubes interact with surfaces much more than with the bulk. The main point of the rheological study [51] was to develop an alternative quantitative (rheological) method of monitoring the state of dispersion.

In order to determine the effect of mixing time on the degree of nanotube dispersion, three identical experiments were performed for samples with 1 wt% concentration of MW nanotubes in PDMS, with the results shown in Fig. 3(a). Each test was conducted on an aliquot of the composite after a certain time of continuous mixing of a sample; this was repeated for three separate mixtures. The values of the viscosity obtained for the short mixing times ($t < 100$ min) have erratic values, such that no trend can be assigned to the viscosity variation with increasing mixing time. This effect is essentially due to jamming of CNT clusters. After a certain time of mixing, these erratic values turn to a consistent value of composite viscosity η, which is the same in different experiments and not much affected by further mixing. This characteristic time, t^*, is interpreted as the minimal time required to achieve the complete dispersion at the given concentration of tubes and the mixing shear stress (which in turn determined by the geometry of shear and the solvent viscosity). Fig. 3(b) illustrates the effect for different CNT concentrations and demonstrates how t^* depends on loading.

From such macroscopic rheological measurements one cannot exclude the presence of consistently small tube clusters, and there is no unambiguous technique to confirm or disprove this in the bulk. A homogeneous dispersion is suggested by images of freeze-fractured surfaces and by comparing the estimates of semiflexible overlap and entanglement concentrations with rheological measurements. For all practical purposes one may regard the sheared composite at $t > t^*$ as completely dispersed, but one must be intentional aware of the length of time required to reach this state.

2.3. *Well-dispersed state,* $t_{mix} > t^*$

The critical time of mixing, t^*, is a function of nanotube concentration and the shear stress in the mixing device (itself a function of vessel geometry and the viscosity of the polymer matrix). The dispersed states have reproducible profile of the rheological linear response. Increasing nanotube concentration increases the values of mixture viscosity η^* and also causes it to become more frequency dependent [51]. Fig. 4 gives a summary of this response in terms of the effective shear modulus of the nanocomposite. The below-overlap 0.5 wt%, 1 wt% and 2 wt% samples, just like the pristine PDMS, exhibit a nearly linear frequency dependence of storage modulus G', which corresponds to the frequency-independent Newtonian viscosity. These systems are dilute enough so that the entanglement between tubes is negligible. There is a significant change in the rheological response between 2 wt% and 4 wt%, which suggests a change in nanocomposite microstructure. Note that these are near the overlap concentration at which one expects the onset of nanotube entanglements in the dispersed state. The emerging rubber plateau with the static gel modulus $G'(\omega \to 0)$ is characteristic for highly entangled CNT dispersions.

Both G' and η^* in the well-mixed state are $\sim$1–2 orders of magnitude lower for the same concentration of nanotubes than the results in earlier literature [52,53]. In view of our findings about the erratic values of response moduli in the state with insufficient tube dispersion (at $t < t^*$), one has to be cautious about the details of preparation of polymer nanocomposites: have the specific polymer nanocomposite been mixed for a sufficient time at a given shear stress of mixing? Such a question is rarely addressed in the current literature, making comparisons difficult.

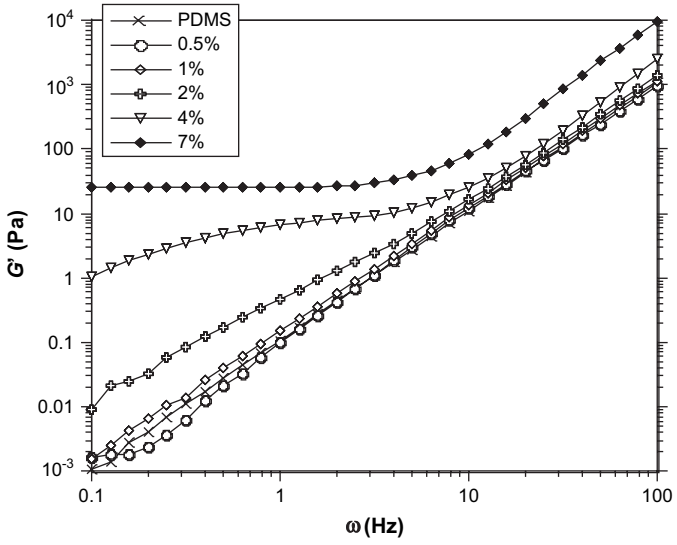

Fig. 4. Frequency dependence of the storage modulus $G'(\omega)$ for well-dispersed samples of different concentrations, also including the pristine PDMS melt. Note the emerging low-frequency rubber plateau at high tube concentrations.

The change in rheological behavior as the concentration of tubes increases, similar to those presented in Fig. 4, has been reported for other CNT/polymer composites and is often called the 'percolation threshold' [52]. More precisely, one might call the emergence of the static gel network the mechanical percolation threshold, to differentiate it from the more traditional electrical percolation [54], or indeed the mathematical problem of percolation of rigid rods [55,56]. Again, there are large discrepancies reported in the literature for such mechanical percolation concentrations, even for the same system. A reason for this might well arise because of two different factors. Firstly, by forming a well-dispersed and homogeneous ($t_{mix} > t^*$) *network* of nanotubes one may reach, and exceed, the entanglement limit. In this case the rheological response would become that of an elastic solid. Secondly, mechanical percolation could take place when individual *aggregates*, or tube clusters (at $t_{mix} < t^*$), come in contact and form force chains. This second type of aggregate-mediated jamming (as well as the electric conductivity threshold) may well be responsible for much higher threshold concentrations previously reported. Better dispersed samples of very long nanotubes will naturally provide much lower percolation thresholds, but also lower effective elastic moduli.

It is important that the emergence of an entangled elastic network of CNTs occurs at concentrations above 2–3 wt%. This agrees favorably with an estimate of overlap concentration based on individual tube parameters, which indicates that the nanotubes are indeed dispersed individually, not in multi-tube bundles. One also finds a characteristic superposition between the mixing time and the frequency of rheological testing, similar to the time/temperature superposition in classical glass-forming polymers [51]. These comparisons provide a proof of complete CNT dispersion, very difficult to obtain otherwise.

3. Actuation of nanotube–polymer composites

For some systems, energy from an external source can trigger changes in the internal state of the structure, leading to a mechanical response much larger than the initial input. The ability to unlock this *internal* work in a solid state structure is of key importance for many potential applications. There are several reports of actuation behavior of nanotube–polymer composites [57–60]. These studies have focussed on accentuating the already present features of the host matrix by adding nanotubes. CNTs acted to exaggerate actuating response by either improving electromechanical properties or increasing heat transfer efficiency due to the inherent high conductivity that originates from their delocalized π-bonded skeleton. We only know of one study that has departed from this traditional 'improvement' scheme and asked whether it was possible to blend nanotubes with benign polymers to create fundamentally new composite properties. Such novel effects have been observed by Courty [61] where electric field stimulation of liquid crystal elastomers with embedded MWCNTs has lead to mechanical contraction. That work was unique in that it details a novel reversible electro-actuator response due to the presence of MWCNTs that otherwise would not occur in that system.

In a series of studies the photomechanical response of MWCNT composites dispersed in a PDMS matrix, subsequently crosslinked into elastomer, has been investigated [27,62–64]. The samples, with a different degrees of CNT alignment induced by pre-stretching, have been illuminated with infrared (IR) light in isostrain conditions, Fig. 5(a). The mechanical stress response to irradiation, and later to switching it off, was very characteristic and fully reversible. Fig. 5(b) shows two possibilities: in elastic composites with CNTs not significantly aligned in any direction, the macroscopic sample shape shows a rapid expansion, which is represented by a rapid drop of measured stress in the constrained geometry. On the other hand, if CNTs are uniaxially aligned, the sample length contracts on irradiation, which shows as a rapid and significant rise in measured stress. The same results were found in other elastomers [62], in particular in natural rubber (sulfur-crosslinked polyisoprene) with dispersed nanotubes. Note that the reversible (i.e. equilibrium) nature of this photomechanical response is in contrast with findings on frequently irreversible loading/unloading/reloading cycles of CNT/elastomer composites, as reviewed in Ref. [22]. We believe in most cases this is a consequence of incomplete CNT dispersion, so that large agglomerates undergo changes under deformation in the matrix.

It is interesting to compare the actuation of carbon nanotube composites with other systems and materials. The famous catalogue of mechanical actuators [65] gives a map of device performances in the plane of actuation stress $\Delta\sigma$ and stroke $\Delta\varepsilon$. At a maximum achieved in Fig. 6(b), $\Delta\sigma \approx 100$ kPa and contractile $\Delta\varepsilon \approx 0.1$ in essentially static conditions, the nanocomposite performance is slightly above the solenoid actuator and almost equal to the human muscle. Taking into account the rates of the effect, discussed below (Fig. 8), in terms of power production these nanocomposites are again placed very near solenoids and muscles on the actuation map.

Also of great interest is the observation that photo-actuation response changes sign at a certain level of pre-strain (at $\varepsilon \sim 10\%$ in Fig. 6). Relaxed or weakly stretched composites show the reversible *expansion* on irradiation, while the same sample, once stretched more significantly, demonstrates an increasing tendency to *contract* along the axis of extension (hence the increase in the measured stress). For comparison, the pristine PDMS rubber in the same experiment shows no discernible photo-stress response at all.

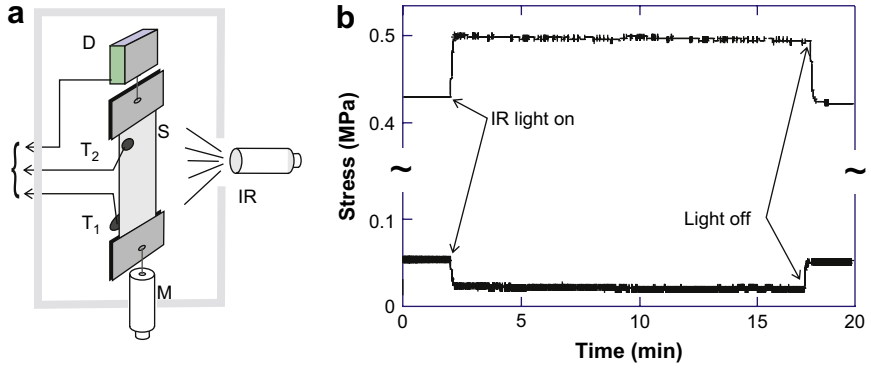

Fig. 5. (a) Scheme of the isostrain setup: the sample (S) is clamped in the frame with its length controlled by the micrometer (M) and the exerted force measured by the dynamometer (D). Thermocouples (T_1 and T_2) are placed in front and behind, on the sample surface to monitor the mean temperature; (b) two characteristic photoelastic response traces. The upper data set is for a well-aligned CNT composite elastomer (under pre-strain of over 40%), which shows the reversible sample contraction on irradiation. The lower set is a non-aligned (weakly stretched) composite, which has its overall length reversibly increasing on irradiation.

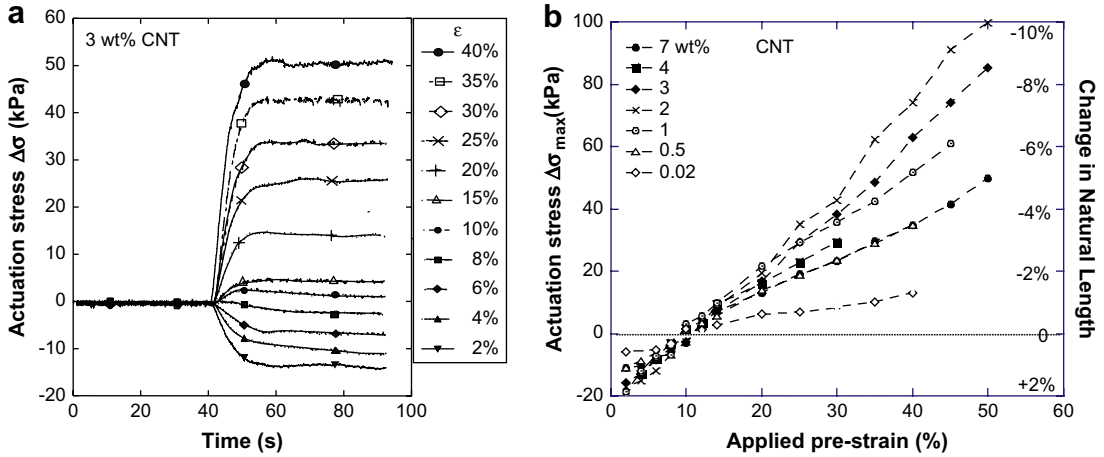

Fig. 6. (a) The actuation stress as a function of time (PDMS elastomer with 3 wt% of MWCNT). Pre-strain ε values (related to the induced tube alignment) are shown in the plot; (b) the maximum, plateau level of actuation stress $\Delta\sigma_{max}$ for different values of pre-strain. The right y-axis shows the corresponding values of actuation stroke representing the change in natural length on irradiation.

One suggestion, arising from these observations, is that a uniaxial pre-strain applied to CNT-loaded elastomers induces an increasing orientational ordering of nanotubes, and this is a primary cause for the change in the nature of their photoelastic response. In fact, there is good evidence that a very good nanotube alignment can be achieved if dispersed in a monodomain liquid crystal elastomer during processing – the mesogenic moieties act to align the tubes [61]. A similar effect has been demonstrated for pure liquid crystals [66,67], and also is known in the field of ferronematics [68]. Although ordinary isotropic polymers are discussed here, clearly the imposed strain will induce some CNT alignment.

3.1. Induced orientation of nanotubes

Let us introduce a simple model based on the affine deformation of the rubbery matrix to estimate the orientational order induced on CNTs by uniaxial stretching. This analysis is broadly based on the arguments presented in Ref. [62]; the reader can also consult Refs. [69–72] where the most straightforward approach is to evaluate the average orientational bias resulting from an imposed uniaxial extension of a matrix, in which the ensemble of rigid rods is initially embedded isotropically. The corresponding orientational order parameter is the average of the second Legendre polynomial of orientation of embedded rods, Fig. 7(a)

$$Q = \int_0^{\pi} \left[\frac{3}{2}\cos^2\theta - \frac{1}{2}\right] P(\theta)\sin\theta \mathrm{d}\theta\mathrm{d}\varphi. \tag{5}$$

Here $P(\theta)$ is the orientational probability distribution, normalized such that $\int P(\theta)\sin\theta\mathrm{d}\theta\mathrm{d}\varphi = 1$. Assuming that the initial state is unaligned, this probability is the flat distribution $P_0(\theta) = 1/(4\pi)$.

The uniaxial extension of an incompressible elastic body is described by the matrix of strain tensor

$$\mathbf{\Lambda} = \begin{pmatrix} 1/\sqrt{\lambda} & 0 & 0 \\ 0 & 1/\sqrt{\lambda} & 0 \\ 0 & 0 & \lambda \end{pmatrix}, \tag{6}$$

where the axis of stretching is taken as z and the magnitude of stretching is measured by $\lambda = 1 + \varepsilon \equiv L/L_0$, the ratio of the stretched and the initial sample length along z, Fig. 7(a). This tensor describes the affine volume-preserving change of shape, which could also be visualized as locally transforming an embedded sphere (representing the orientational distribution P_0) into an ellipsoid (representing the induced orientational bias) of the same volume and the aspect ratio $R_{\|}/R_{\perp} = \lambda^{3/2}$.

After such a deformation, every element of length in the body changes affinely according to the matrix product $\boldsymbol{L}' = \mathbf{\Lambda}\cdot\boldsymbol{L}$, which in our case of uniaxial incompressible extension means that

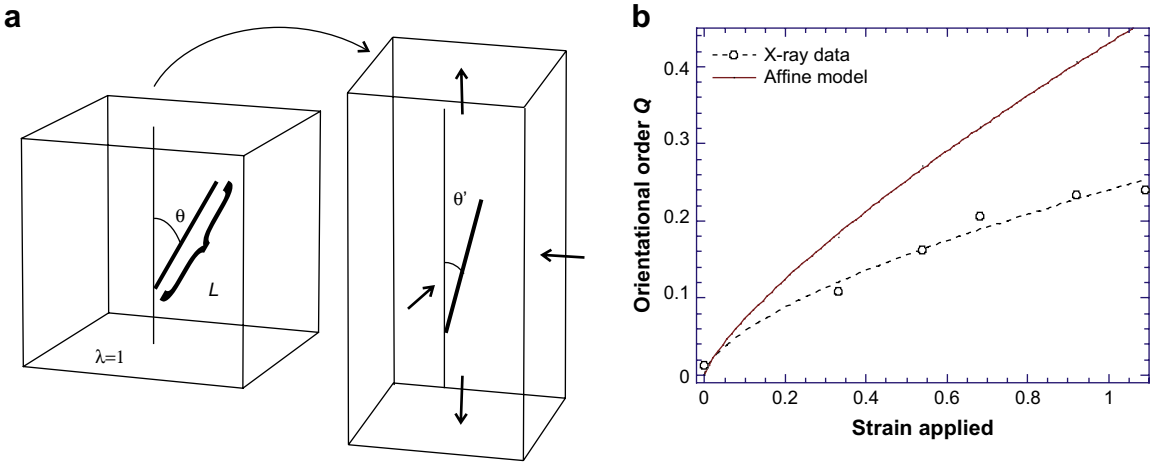

Fig. 7. (a) The scheme of an affine incompressible extension, changing the orientation of an inflexible rod embedded in a continuous medium; (b) the change in the orientational order parameter Q of nanotubes in response to the imposed uniaxial strain $\varepsilon = \lambda - 1$. Solid line shows the affine rigid rod model prediction, data points ○ present an experimental measurement (dashed line is a guide to the eye).

$L'_z = \lambda L_z$ and $L'_\perp = (1/\sqrt{\lambda})L_\perp$. This corresponds to the new angle of the rod, θ' such that $\tan\theta' = L'_\perp/L'_z = (1/\lambda^{3/2})\tan\theta$. Therefore, to obtain the new (now biased) orientational distribution function we need to convert the variable θ into the new (current) variable θ', which gives

$$\theta \rightarrow \arctan\left(\lambda^{3/2}\tan\theta'\right);$$
$$\sin\theta \mathrm{d}\theta \rightarrow \frac{\lambda^3}{\left(\cos^2\theta' + \lambda^3\sin^2\theta'\right)^{3/2}}\sin\theta' \mathrm{d}\theta'. \quad (7)$$

This defines the expression for the normalized orientational distribution function

$$P(\theta') = \frac{\lambda^3}{4\pi\left(\cos^2\theta' + \lambda^3\sin^2\theta'\right)^{3/2}}, \quad (8)$$

which is an explicit function of the uniaxial strain applied to the body and can be used to calculate the induced order parameter Q:

$$Q(\varepsilon) = \frac{3}{2}\int \frac{\cos^2\theta'[1+\varepsilon]^3\sin\theta' \mathrm{d}\theta' \mathrm{d}\varphi}{4\pi\left(\cos^2\theta' + [1+\varepsilon]^3\sin^2\theta'\right)^{3/2}} - \frac{1}{2}. \quad (9)$$

Analytical integration of this expression gives an explicit function $Q(\varepsilon)$ [62], which is plotted as a solid line in Fig. 7(b). At relatively small strains, it approaches the linear regime: $Q \approx (3/5)\varepsilon - (6/35)\varepsilon^2 + \ldots$.

Fig. 7(b) compares the results of the calculation of $Q(\varepsilon)$, acquired as a function of sample strain applied to an initially isotropic sample, with the experimental data [62] obtained by X-ray scattering of stretched nanocomposites (7 wt% CNT in PDMS). On stretching, substantial values of induced orientational order have been reached. Furthermore, the change in orientation on stretching was reversible, i.e. equilibrium, with orientational order parameter returning back to zero with the imposed strain removed. Evidently, the experimental data display a lower order parameter than that predicted by the affine model, although has the same qualitative trend. One must remember that this simple model does not account for tube flexibility. Also, some proportion of the tubes would be unable to rotate affinely due to the entanglements. The experimental data reflect this and, accordingly, gives slightly lower values of order parameter.

3.2. Mechanisms of photo-actuation

There is still no full understanding of nanotube photomechanical behavior when embedded in a host polymer matrix, because to a large degree, no noninvasive and nondestructive technique is available to monitor their state. The results apparently do not depend on the host matrix, suggesting that the nanotube filler units are indeed the origin of the observed actuation response. Photon absorption produced a response from the tubes, which directly translated into the macroscopic effect in an otherwise benign polymer system.

The data in Fig. 8 are presented to demonstrate the speed of the actuation process more clearly and also differentiate between the light and heat-driven actuation mechanisms. The change in stress and change in temperature are plotted, normalized by their maximal value at saturation in the given experiment; plotted in this form, all the results (for different tube loading and different pre-strain) appear universal [63].

The change in temperature by IR-heating is unavoidable and reaches $\Delta T \sim 15\,^\circ$C maximally on the sample surface. This highlights an important question as to whether the mechanical response is due to the photon absorption or plain heat. Fig. 8(a) shows that the stress reaches its peak and saturation in $\sim$10 s, while the temperature takes over 2 min to reach its peak. Although the difference in rates is not very dramatic, the fact that the stress response is faster suggests that its mechanism is not caused by the trivial heating. In a separate study the conclusion was reached that thermo-mechanical effects do exist (i.e. the MWCNT-loaded composite has a stronger mechanical response to heating than a pristine polymer) but the magnitude is almost a decade smaller than the direct IR-photon absorption mechanism. There is also an interesting question of what role might be played by the temperature gradient across the sample thickness, which would cause a dynamic bending in a free sample. A recent work has discussed the kinetics of heat diffusion and associated inhomogeneous strains in such situation [73]. However, the results discussed here are for isostrain sample confinement and the temperature may only have an effect averaged over the thickness.

The behavior was repeatable for all nanotube–polymer concentrations. For reference, Fig. 8(b) also presents the results for the pristine PDMS elastomer (no photomechanical response) and the composite with very low tube concentration, 0.02 wt%. The notably

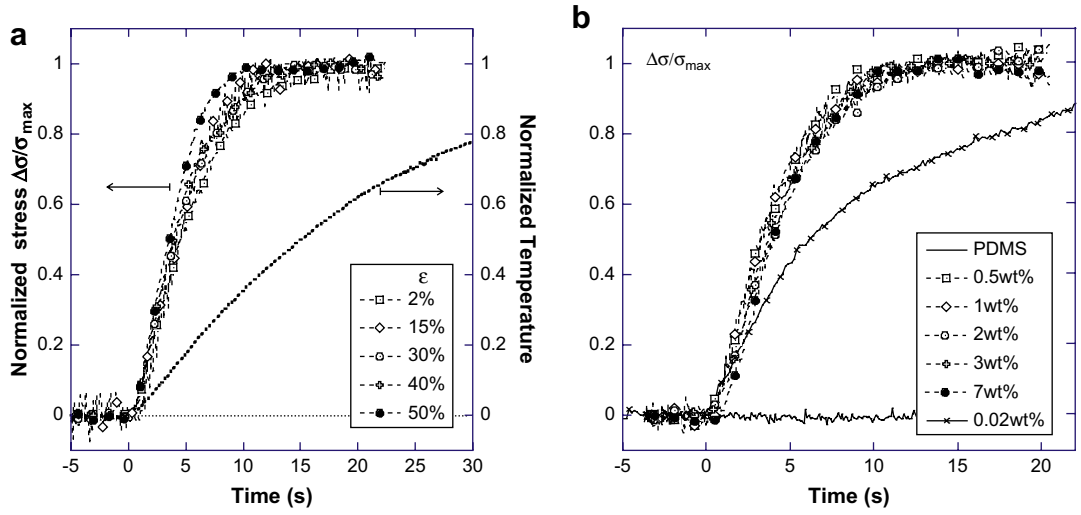

Fig. 8. Normalized stress, $\Delta\sigma/\sigma_{max}$ vs. time, which allows comparison of the response kinetics: (a) the light-on response of 3 wt% PDMS composite at different values of pre-strain ε. The right y-axis shows the simultaneously measured, similarly normalized, change in temperature on irradiation; (b) the light-on response of different composites, all at the same 20% pre-strain.

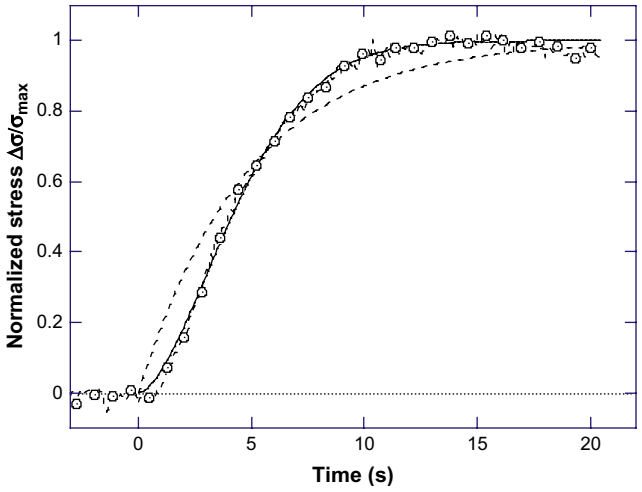

Fig. 9. Illustration of the data fit, for a 3 wt% composite at 20% pre-strain. Experimental data (○) are fitted by the compressed-exponential (solid line) and the simple exponential (dashed line) to demonstrate the discrepancy. All data sets in Fig. 8 are fit with the same compressed-exponential function.

slower response of this sample is in marked contrast to all other composites. This discrepancy will present the greatest difficulty when attempting to offer an explanation for the observed effects.

Examining the time dependence of the photo-response, the data have been fitted with a compressed-exponential function $1-\exp[-(t/\tau)^{\beta}]$. The quality of this fit, as well as the important comparison with the classical exponential behavior, are shown in Fig. 9. The two fitting parameters are the relaxation time, $\tau \approx 5$ s and the exponent $\beta \approx 2$ [63]. These values were the same for all aligned composites with nanotube concentrations above the percolating threshold. It is prudent to focus on the main effect and disregard a weak dependence of τ and β on the applied pre-strain, suggested by Fig. 8(a). Such a fast response of the system is a striking result. One must appreciate that the individual photomechanical response of a free-standing nanotube must proceed within a nanosecond timescale, if one assumes polaron excitation and relaxation [74]. The relatively slow kinetics at the scale of seconds is certainly due to the rubbery matrix constraints. The polymer would usually be expected to follow the classical Debye relaxation (corresponding to $\beta = 1$), if not slower due to the mode coupling and viscoelasticity. This is not the case in these experiments where the compressed exponent $\beta \approx 2$ is evidently the result, cf. Fig. 9. Moreover, the fast cooperative response is reproduced in both expansive (unaligned) and contractive (aligned) modes of photo-actuation, suggesting a unique underlying mechanism for the bimodal photomechanical effect.

When the light source is switched off, Fig. 10(a), all the nanocomposite materials in the given range relax normally, following the classical $e^{-t/\tau}$ law with $\tau \approx 5$ s. The same normalized kinetics of the light-off relaxation is obtained at all different values of pre-strain ε. As a more detailed comparison to the fast light-on response, the plot in Fig. 10(b) shows results from an identical experiment conducted on PDMS-dispersed composites with trace amounts of nanotubes (0.02 wt%) and also with 3 wt% of an ordinary carbon black. The response is evidently much slower in this case. Importantly, these curves superpose and also follow a simple exponential fit, $1-e^{-t/\tau}$, with $\tau \approx 10$ s here (also much lower amplitude, as discussed above). Evidently, for the faster response to take place, nanotube (and not carbon black) concentration needs to remain above the percolating threshold.

Apart from the ideas based on the electronic structure of nanotubes, there is another possibility to account for their apparent large local deformation in a polymer matrix. A large (and fast) local tube heating is inevitable on photon absorption. In fact, there are reports of such an effect [59,75], presumably based on the incomplete re-radiation of the absorbed energy. Assuming the polymer chains are highly aligned in the vicinity of nanotubes due to the boundary anchoring on their surface, the local heating should generate local contracting strain along the alignment axis. This is a classical thermodynamic effect of uniaxial contraction of a stretched rubber. Such a local strain could lead to an Euler buckling instability of a rigid nanotube embedded in the elastic matrix, which would account for many features of photo-actuation.

Consider now the dynamics of such a response, assuming the relaxation process is controlled by the overdamped balance of an elastic force against viscous friction. To understand the fast response one must take the observed time dependence $x \sim \exp[-\alpha t^2]$, where $x(t)$ is the relevant strain variable, and work backwards to isolate the nature of the forces involved. Taking $\ln x = -\alpha t^2$ and differentiating, one obtains the 'kinetic equation' in the form $\dot{x} = -(2\alpha t)x$. The effective relaxation time has to be the ratio of the elastic modulus G to the viscous coefficient η, from the force balance $Gx + \eta\dot{x} = 0$. In order to generate the compressed-exponential, this ratio $[G/\eta]$ has to be a linear function of time since the moment the light was switched on.

On sudden local heating, the equilibrium balance between the chain alignment and the boundary conditions on the tube surface is

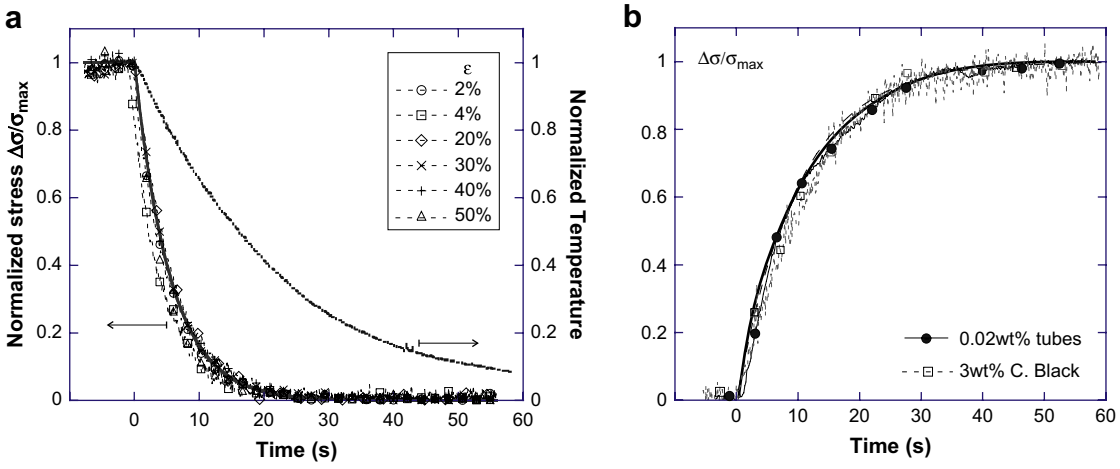

Fig. 10. (a) The normalized stress relaxation of a 3 wt% nanocomposite illuminated at different pre-strain, when the light source is switched off. The right *y*-axis shows the simultaneously measured, similarly normalized, change in temperature on irradiation; (b) the light-on response of the composite with very low tube loading, and also that of a sample with 3 wt% carbon black, both at $\varepsilon = 20\%$. The Debye relaxation is found in both cases, with the fit curve shown by the solid line in both the plots.

distorted: the entropy cost for chain stretching increases, resulting in a uniaxial contracting force exerted on the tube along its axis. The magnitude of this force, in the leading order, is a linear function of the local temperature increase $\Delta T = T(t) - T_0$. If the temperature increases, then the contracting force would increase as a function of time too (initially – linearly with time). In small increments at $t \to 0$ we can write $G = g_0 t$ and the kinetic equation becomes $\dot{x} = -[g_0/\eta]tx$, exactly reproducing the results of our observations, with the effective relaxation time $\tau = \eta/g_0 t$.

Of course, there are many complications to this simple model. For instance, the viscosity in the dissipating medium is also a function of temperature (in simplest terms, proportional to the Arrhenius activation, $\eta \propto e^{E/kT}$); this will introduce an additional time dependence $\eta \approx \eta_0(1 - at)$. The real viscoelasticity of a polymeric system would make all of these estimates much more complicated. However, in the leading order, one would still expect to see the contraction dominated by the linear (or near-linear) time dependence of the local rubber modulus.

The fast compressed–exponential response was not found in the light-off relaxation, which agrees with the basic logic presented here. After the illumination period, the temperature equilibrates through the whole sample, giving the average temperature that is detected. The new balance of forces is reached, maintained by the steady flux of heat from the irradiated tubes. When the light is turned off, both the viscosity and the modulus remain roughly constant (only weakly dependent on time), resulting in the simple Debye relaxation towards the original local conformation of the elastomer which was established at the crosslinking.

4. Carbon nanotube mats and fibers

The attempted explanation of photo-actuation in CNT composite elastomers, based on the sharp local heating of nanotubes, captures many key features of the findings, but also has some difficulties in describing CNT concentrations well below overlap. For some reason, only the higher-concentration CNT composites with tubes forming the entangled network inside the polymer matrix, display the fast reversible photo-actuation. In order to try and separate the effects of CNTs from the effects of the polymer matrix, albeit stimulated by the tube presence, the recent study has examined the same photomechanical effect in pure nanotube mats and fibers [46,76].

Indeed, one can ask a very real question: do carbon nanotubes behave like polymers? This essentially questions the role of thermal fluctuations and ergodicity, so dominant in polymer science, when they are applied to nanotubes. The answer appears to be – some do and some do not, depending on the number of walls. Analyzing the behavior of carbon nanotube networks, as found in sheets of SW or MWCNTs (often called 'bucky-paper' [77–79]) provides an intriguing insight into the characteristics of nanotubes, non-invasively deducing the fundamental response of individual tubes from the average characteristics of the collective. The fundamental issue is whether the tubes behave as static elastic (or indeed plastic) rods, or they are able to explore their available conformational space like thermally fluctuating polymer chains. The secondary question is about the nature of linkages in such nanotube networks. One should not confuse this issue with the volume of successful literature describing the mechanical response of individual nanotubes, such as their static Young modulus: here we discuss the dynamic-mechanical properties of nanotube networks either under stress, or when heat or light stimulus is applied.

Long-time stress relaxation experiments on such nanotube networks have been reported in Ref. [46]. When a small step-strain is applied to a sample of viscoelastic material, the characteristic stress relaxation takes place, in effect, the recording of stress against time returns the value of Young (extensional) elastic modulus. This is a

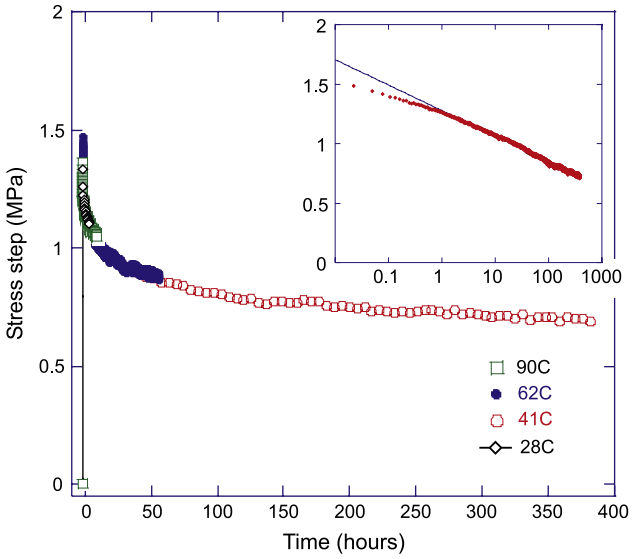

Fig. 11. Stress relaxation of a MWCNT network kept at fixed length, after a step-strain of 0.2%. Different data sets, obtained at 28 °C, 41 °C, 60 °C and 90 °C are color-coded. The inset shows the fitting with the logarithmic relaxation function.

classical isostrain experiment in viscoelastic medium, schematically shown in Fig. 5(a). The nature of stress relaxation process, when observed over an extended time, reveals many details of the viscoelasticity of the material. Experimental similarities between MWCNT networks and a 'sticky' granular system have been observed, in the sense of both being completely non-thermal. In contrast, SWCNTs display thermally-driven entropic properties akin to a rubber network. Since SWCNTs practically never exist in a form of a network with crossing contacts (certainly not in the case studied [46,76]), this suggests that the thick SWCNT bundles are in fact quite dynamic and undergo a thermal bonding–debonding process.

The analysis of MWCNT data in Fig. 11 suggests a very slow but remarkably large amplitude of stress relaxation. The inset illustrates the same data plotted on the logarithmic time-axis, which highlights how the best power-law fit deviates from the data more significantly, while the logarithmic relaxation given by $\Delta\sigma\,(\mathrm{MPa}) \approx 1.3–0.2 \ln t$ fits the experimental results almost perfectly after the first hour of relaxation. Such a slow dynamics is very rare in physics and resembles the finding in overconstrained randomly quenched systems. It is found, for instance, in the relaxation of the angle of repose in a sandpile [80] or in polydomain nematic elastomers [81]. In each case it is the network of quenched mechanical constraints that leads to the exponential increase in the activation barrier as the equilibrium approaches, and a logarithmic relaxation as a result.

In an identical step-strain experiment at different temperatures, SWCNT network responds in a marked contrast to multi-walled case. Fig. 12 shows that at any stage of relaxation, the stress in a stretched SWCNT network is higher as the temperature is increased. The corresponding elastic modulus reproduces the classical feature of rubber elasticity: the linear dependence of the modulus on absolute temperature. This implies the entropic nature of SWCNT network: unlike in MWCNT case, thermal fluctuations are in fact significant. However, this conclusion has to be taken together with the well-established bundled nature of SWCNT assemblies, very different from the coiled polymer chains. As single-wall tubes are flexible enough to be thermally excited, they assemble in highly aligned bundles held by van der Waals forces, but dynamic in the sense that their range of conformations is explored under thermal motion of continuously bonding and debonding flexible tubes. The corresponding entropy would then account for the temperature-dependent modulus (analogous to polymer networks where the

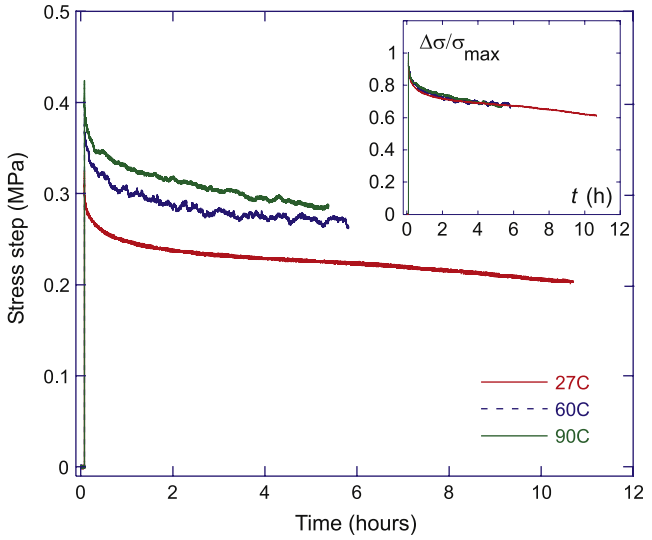

Fig. 12. Stress relaxation of a SWNT mat kept at fixed length, after a step-strain of 0.2%. The modulus depends linearly on absolute temperature at all times of relaxation. However, the inset displays the normalized data $\Delta\sigma/\Delta\sigma_{max}$, indicating the universal relaxation mechanism, not altered with temperature.

coiled chains between junctions are exploring their conformational freedom). The MWCNT strands are much more rigid and not able to bend under thermal excitation so that the structure of their networks is entirely dependent on preparation history.

Another key finding points at the difference between entropic polymer and entropic SWNT bundles. The inset in Fig. 12 shows the normalized stress relaxation, rescaled by $\Delta\sigma/\Delta\sigma_{max}$, helping to clarify the long-time relaxation mechanism of SWCNT networks. The normalized curves collapse onto each other suggesting that the mechanism of stress relaxation is the same regardless of temperature, just like in MWCNT case. This is not the case for a crosslinked polymer network where relaxation is a diffusion-controlled process and hence its rate varies with T (leading to the famous time/temperature superposition). Non-thermal relaxation in nanotube networks suggests that the main mechanism is novel. We believe that it is related to the sliding of junctions between nanotubes, which is dominated by friction. The rate of long-time normalized relaxation of stress is much faster in SWCNT networks: this is in line with the idea of sliding junction, as the binding energy is certainly proportional to the nanotube dimensions.

The mechanical response of nanotube networks to near-IR light is very similar to what was reported in polymer composites. The use of a cold light source is an effective means to remotely transfer energy to the system quickly. In experiments, following the same setup as shown in Fig. 5(a), the photo-induced stress response was recorded and presented in Fig. 13. For MWCNT mat, the significant drop in stress indicates that the sample expands its underlying natural length on irradiation. The expansion is fully reversible, as the sample returns to its original stressed state on removing the source of external energy, Fig. 13(a). This is a very important observation, eliminating many possible mechanisms based on tube degradation, induced defects, or enhanced junction sliding, which would all be irreversible. Characteristically, the kinetics of this photomechanical response is very slow, although at least 1–2 orders of magnitude faster than the ambient stress relaxation, Fig. 11. There is a small but significant and reproducible contraction in the initial seconds after the light source is switched on, highlighted in the inset. Similarly, when the light is switched off, the same magnitude peak in opposite direction was observed. This feature needs to be compared with the response of SWCNT mat to irradiation, Fig. 13(b). Clearly SWCNTs contract under IR radiation, leading to the increasing stress on the constrained sample. The effect is also fully reversible and its relatively fast kinetics is illustrated in the inset.

The SWCNT network contraction on irradiation matches well with our earlier discussion on their thermal (entropic) nature. We must consider the effect of stretched rubber band contraction on heating, which is due to the increasing weight of conformational entropy. As this is a significant factor in the description of SW tubes and their bundles, one expects as in classical thermodynamics that $(\partial f/\partial T)_x = (\partial S/\partial x)_T$, with x the stretching and f the corresponding force. This basic consequence of entropic elasticity is almost completely independent on what actual graphene lattice does microscopically. In both SW and MWCNT cases, photo-stimulated actuation is orders of magnitude larger than thermal expansion predictions for individual nanotubes, suggesting a new paradigm for theoretical and experimental studies.

5. Conclusions

In this review a brief survey of the polymer–nanotube composites has been given, with particular emphasis on the physics underpinning this new frontier of materials research. Post-production dispersion techniques for CNTs with no particular surface

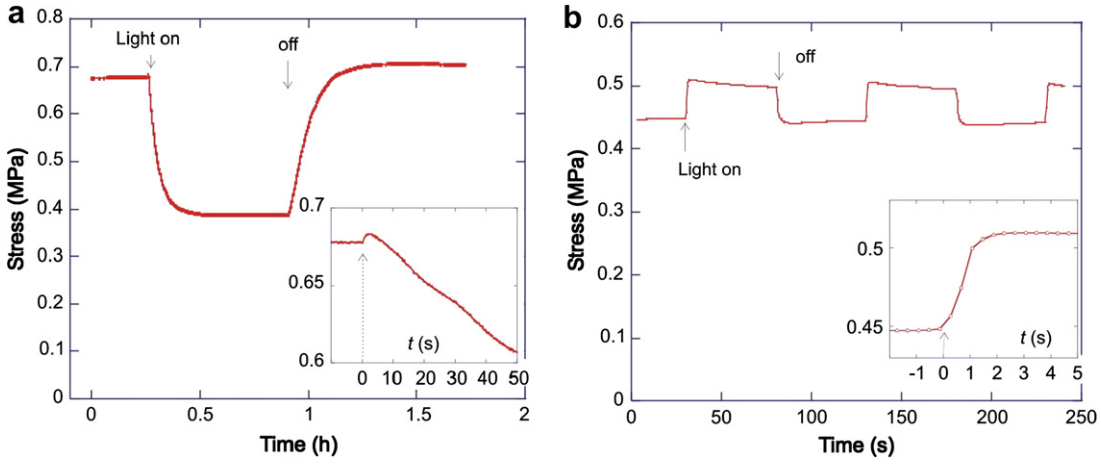

Fig. 13. (a) Photomechanical actuation of MWCNT mat recorded at fixed sample length. The inset shows the initial contractive stress response of the film during the first few seconds when the light source is switched on; (b) photomechanical response of SWNT mat, in the same conditions, shows the sample contracting on illumination. The detailed onset kinetics, highlighted in the inset, matches well the compressed-exponential kinetics [63].

functionalization have been discussed, followed by a considerable detail given over to the mechanical actuation properties and mechanisms which have recently been discovered in these systems.

Comparing the estimates of VDW interaction and shear forces suggest that only at sufficiently high shear energy density one can hope to achieve dispersion of CNT agglomerates arriving from production lines. This high energy density is easily achieved during ultrasonic cavitation, which requires low-viscosity solvents and great care to avoid significant tube damage. In this context, we offered a simple theoretical model, based on affine radial flow, to estimate the characteristic nanotube length L_{lim} below which the cavitation-driven scission does not occur.

In contrast, in shear mixing devices one must aim for high-viscosity polymer solutions or melts, however, in any case it is unlikely that parallel CNT bundles could be separated by shear mixing. Experiments have shown that a critical time t^* is needed to disperse carbon nanotubes in a polymer melt, reaching a consistent and reproducible state of such a dispersion. Below this characteristic time, the composite system is full of dense tube clusters (often smaller than an optical microscope resolution). This manifests itself in erratic rheological properties, depending on accidental jamming of the resulting "colloidal glass". Dispersions mixed for a time longer than t^* appear homogeneously mixed. One cannot exclude the presence of consistently small tube clusters or bundles, and there is no unambiguous technique to confirm or disprove this. However, a homogeneous dispersion is suggested by images of freeze-fractured surfaces reported in the literature, and by comparing the estimates of semiflexible overlap and entanglement concentrations with rheological measurements of dispersed composites.

Nanotube overlap is a very important parameter in nanocomposites. Well-dispersed systems possess very different rheological properties below and above the concentration of "mechanical percolation" (we use this term reluctantly, only because it seems to be in heavy use in the literature: the true percolation is a somewhat different physical process [55,56]). At low concentrations, non-interacting nanotubes homogeneously dispersed in the polymer matrix take a very long time to re-aggregate, provided the matrix viscosity is high enough to suppress fast Brownian motion (or crosslinked into elastomer after dispersion). The rheology of such dispersions remains that of a viscous liquid, or classical rubber, with the response a linear function of tube concentration. At concentrations above the threshold of order $n_c \sim 2$–3 wt% in the case discussed here, there is a clear emergence of an elastic gel of entangled nanotubes in their homogeneously dispersed state. The rheological characteristics of these composites with entangled CNTs are reported to have a distinct rubber modulus G' at low frequencies. There is also a characteristic superposition between the mixing time and the frequency of rheological testing, similar to the time/temperature superposition in classical glass-forming polymers.

Elastomers filled with nanotubes respond to light with a significant mechanical actuation. The strength of photomechanical response is of the order of tens of kiloPascals. Translated into the stroke, this corresponds to actuation strains of $+2$ (expansion) to -10% (contraction) depending on the CNT concentration and alignment in the host matrix. At the same time, differing host polymers are reported to have a relatively neutral role in the actuation mechanism. Importantly, the kinetics of this photo-actuation is much faster than that classical relaxation predicts, following a compressed-exponential law.

Understanding the nature of the actuator mechanisms in nanocomposites certainly warrants further theoretical and experimental investigation. Many questions remain completely unclear. One possible explanation discussed here considers CNTs as photon absorbers that locally redistribute the energy as heat causing contraction of anisotropic polymer chains aligned near the nanotube walls. This demonstrates how nanotubes could impart new properties to otherwise benign materials; the role of the nanotube–polymer interface is of great interest and the speed of the photo-actuation response warrants much further experimental and theoretical investigation.

Networks of carbon nanotubes may be the first system that exhibits metallic, semiconducting and polymer-like properties within one material – and apparently also demonstrate a reversible light-induced actuation, almost four decades larger than what would be expected through lattice thermal expansion/contraction arguments. On/off hysteresis is also negligible. Better aligned MWCNT systems such as that found in twisted fibers unambiguously show nanotube contraction along the alignment axis. SWCNT networks always contract in the direction of pre-strain. As single-walled CNT films appear to behave like crosslinked polymer systems, crosslinking the individual SWCNTs chemically may very well create a pure nanotube elastomer with some intriguing properties.

A huge international research effort is ongoing to quantify the properties and the science of polymer–nanotube composites. This is an exciting time to be involved in the field with new fundamental discoveries occurring regularly. It is hoped that this review will contribute in some small way to future discoveries and will inspire new research to augment an already fruitful discipline.

Acknowledgments

We thank S.F. Edwards, A.M Squires and A.R. Tajbakhsh for insightful discussions. Help and advise of O. Trushkevich, B. Panchapakesan and A. Ferrari are gratefully appreciated. Parts of this work have been supported by EPSRC, ESA-ESTEC (18351/04), The Gates Foundation and Makevale Ltd.

References

[1] Mathews FL, Rawlings RD. Composite materials: engineering and science. Chapman and Hall; 1994.
[2] Milton GW. The theory of composites. Cambridge University Press; 2002.
[3] Dresselhaus MS, Dresselhaus G, Sugihara K, Spain IL, Goldberg HA. In: Gonser U, editor. Graphite fibers and filaments. Berlin: Springer; 1988.
[4] Arpe HJ. Ullmann's encyclopedia of industrial chemistry. Wiley; 1998.
[5] Rodriguez NM. A review of catalytically grown nanofibers. J Mater Res 1993;8:3233–50.
[6] Chung D. Carbon fiber composites. NY: Butterworth-Heinemann; 1994.
[7] Ajayan PM, Ebbesen TW. Nanometer-size tubes of carbon. Rep Prog Phys 1997;60:1025–62.
[8] Iijima S. Helical microtubules of graphitic carbon. Nature 1991;354:56–8.
[9] Tennent HG. Carbon fibrils, method for producing same and compositions containing same. US Patent 4663230; May 5th, 1987.
[10] Endo M. Mechanisme de croissance en phase vapeur de fibres de carbone (the growth mechanisms of vapour-grown carbon fibers). PhD Thesis; 1975.
[11] Ajayan PM, Iijima S. Smallest carbon nanotube. Nature 1992;358:23.
[12] Iijima S, Ichihashi T. Single-shell carbon nanotubes of 1-nm diameter. Nature 1993;363:603–5.
[13] Bethune D, Kiang C, Devries M, Gorman G, Savoy R, Vazquez J, et al. Cobalt-catalyzed growth of carbon nanotubes with single-atomic-layerwalls. Nature 1993;363:605–7.
[14] Ajayan PM, Stephan O, Colliex C, Trauth D. Aligned carbon nanotube arrays formed by cutting a polymer resin-nanotube composite. Science 1994;265:1212–4.
[15] Wagner HD, Lourie O, Feldman Y, Tenne R. Stress-induced fragmentation of multiwall carbon nanotubes in a polymer matrix. Appl Phys Lett 1998;72:188–91.
[16] Lourie O, Cox DM, Wagner HD. Buckling and collapse of embedded carbon nanotubes. Phys Rev Lett 1998;81:1638–42.
[17] Curran SA, Ajayan PM, Blau WJ, Carroll DL, Coleman JN, Dalton AB, et al. A composite from poly(*m*-phenylenevinylene-*co*-2,5-dioctoxy-*p*-phenylenevinylene) and carbon nanotubes: A novel material for molecular optoelectronics. Adv Mater 1998;10:1091–3.
[18] Schadler LS, Giannaris SC, Ajayan PM. Load transfer in carbon nanotube epoxy composites. Appl Phys Lett 1998;73:3842–5.
[19] de Heer W. Nanotubes and the pursuit of applications. MRS Bull 2004;29:281–5.

[20] Curran S, Davey AP, Coleman J, Dalton A, McCarthy B, Maier S, et al. Evolution and evaluation of the polymer nanotube composite. Synth Met 1999;103:2559–62.
[21] Giordani S, Bergin SD, Nicolosi V, Lebedkin S, Kappes MM, Blau WJ, et al. Debundling of single-walled nanotubes by dilution. J Phys Chem B 2006;110:15708–18.
[22] Bokobza L. Multiwall carbon nanotube elastomeric composites: a review. Polymer 2007;48:4907–20.
[23] Shi DL, Feng XQ, Huang YGY, Hwang KC, Gao HJ. The effect of nanotube waviness and agglomeration on the elastic property of carbon nanotube-reinforced composites. J Eng Mater Technol 2004;126:250–7.
[24] Onsager L. The effects of shape on the interactions of colloidal particles. Ann NY Acad Sci 1949;51:627.
[25] De Gennes PG. A semi-fast artificial muscle. Compt Rend Acad Sci Serie IIB 1997;324:343–8.
[26] Lu S, Panchapakesan B. Nanotube micro-optomechanical actuators. Appl Phys Lett 2006;88:253107.
[27] Ahir SV, Terentjev EM. Photomechanical actuation in polymer–nanotube composites. Nature Mater 2005;4:491–5.
[28] Girifalco LA, Hodak M, Lee RS. Carbon nanotubes, buckyballs, ropes, and a universal graphitic potential. Phys Rev B 2000;62:13104–10.
[29] Strano M, Moore VC, Miller MK, Allen M, Haroz E, Kittrell C, et al. The role of surfactant adsorption during ultrasonication in the dispersion of single-walled carbon nanotubes. J Nanosci Nanotechnol 2003;3:81–6.
[30] Moniruzzaman M, Winey KI. Polymer nanocomposites containing carbon nanotubes. Macromolecules 2006;39:5194–205.
[31] Hilding J, Grulke EA, Zhang ZG, Lockwood F. Dispersion of carbon nanotubes in liquids. J Dispersion Sci Tech 2003;24:1–41.
[32] Thess A, Lee R, Nikolaev P, Dai HJ, Petit P, Robert J, et al. Crystalline ropes of metallic carbon nanotubes. Science 1996;273:483–7.
[33] Shvartzman-Cohen R, Nativ-Roth E, Baskaran E, Levi-Kalisman Y, Szleifer I, Yerushalmi-Rozen R. Selective dispersion of single-walled carbon nanotubes in the presence of polymers: the role of molecular and colloidal length scales. J Am Chem Soc 2004;126:14850–7.
[34] Paulusse JMJ, Sijbesma RP. Ultrasound in polymer chemistry: revival of an established technique. J Polym Sci Part A Polym Chem 2006;44:5445–53.
[35] Gedanken A. Sonochemistry and its application to nanochemistry. Curr Sci 2003;85:1720–2.
[36] Lohse D. Sonoluminescence – cavitation hots up. Nature 2005;434:33–4.
[37] Birkin PR, Offin DG, Joseph PF, Leighton TG. Cavitation, shock waves and the invasive nature of sonoelectrochemistry. J Phys Chem B 2005;109:16997–7005.
[38] Nguyen TQ, Liang OZ, Kausch HH. Kinetics of ultrasonic and transient elongational flow degradation: a comparative study. Polymer 1997;38:3783–93.
[39] Chen GX, Li YJ, Shimizu H. Ultrahigh-shear processing for the preparation of polymer/carbon nanotube composites. Carbon 2007;45:2334–40.
[40] Kuijpers MWA, Iedema PD, Kemmere MF, Keurentjes JTF. The mechanism of cavitation-induced polymer scission; experimental and computational verification. Polymer 2004;45:6461–7.
[41] Lu KL, Lago RM, Chen YK, Green MLH, Harris PJF, Tsang SC. Mechanical damage of carbon nanotubes by ultrasound. Carbon 1996;34:814–6.
[42] Martinez MT, Callejas MA, Benito AM, Cochet M, Seeger T, Anson A, et al. Sensitivity of single wall carbon nanotubes to oxidative processing: structural modification, intercalation and functionalisation. Carbon 2003;41:2247–56.
[43] Xing YC, Li L, Chusuei CC, Hull RV. Sonochemical oxidation of multiwalled carbon nanotubes. Langmuir 2005;21:4185–90.
[44] Hennrich F, Krupke R, Arnold K, Stutz JAR, Lebedkin S, Koch T, et al. The mechanism of cavitation-induced scission of single-walled carbon nanotubes. J Phys Chem B 2007;111:1932–7.
[45] Badaire S, Poulin P, Maugey M, Zakri C. In situ measurements of nanotube dimensions in suspensions by depolarized dynamic light scattering. Langmuir 2004;20:10367–70.
[46] Ahir SV, Terentjev EM, Lu SX, Panchapakesan B. Thermal fluctuations, stress relaxation, and actuation in carbon nanotube networks. Phys Rev B 2007;76:165437.
[47] Shvartzman-Cohen R, Levi-Kalisman Y, Nativ-Roth E, Yerushalmi-Rozen R. Generic approach for dispersing single-walled carbon nanotubes: the strength of a weak interaction. Langmuir 2004;20:6085–8.
[48] Pestman JM, Engberts JBFN, DeJong F. Sonochemistry – theory and applications. Recl Trav Chim Pays-Bas 1994;113:533–42.
[49] Katoh R, Tasaka Y, Sekreta E, Yumura M, Ikazaki F, Kakudate Y, et al. Sonochemical production of a carbon nanotube. Ultrason Sonochem 1999;6:185–7.
[50] Wang Y, Wu J, Wei F. A treatment method to give separated multi-walled carbon nanotubes with high purity, high crystallization and a large aspect ratio. Carbon 2003;41:2939–48.
[51] Huang YY, Ahir SV, Terentjev EM. Dispersion rheology of carbon nanotubes in a polymer matrix. Phys Rev B 2006;73:125422.
[52] Potschke P, Fornes TD, Paul DR. Rheological behavior of multiwalled carbon nanotube/polycarbonate composites. Polymer 2002;43:3247–55.
[53] Song WH, Windle AH. Isotropic-nematic phase transition of dispersions of multiwall carbon nanotubes. Macromolecules 2005;38:6181–8.
[54] Du FM, Scogna RC, Zhou W, Brand S, Fischer JE, Winey KI. Nanotube networks in polymer nanocomposites: rheology and electrical conductivity. Macromolecules 2004;37:9048–55.
[55] Bug ALR, Safran SA, Webman I. Continuum percolation of rods. Phys Rev Lett 1985;54:1412–5.
[56] Vigolo B, Coulon C, Maugey M, Zakri C, Poulin P. An experimental approach to the percolation of sticky nanotubes. Science 2005;309:920–3.
[57] Landi BJ, Raffaelle RP, Heben MJ, Alleman JL, VanDerveer W, Gennett T. Single wall carbon nanotube–nafion composite actuators. Nano Lett 2002;2:1329–32.
[58] Tahhan M, Truong VT, Spinks GM, Wallace GG. Carbon nanotube and polyaniline composite actuators. Smart Mater Struct 2003;12:626–32.
[59] Koerner H, Price G, Pearce NA, Alexander M, Vaia RA. Remotely actuated polymer nanocomposites – stress-recovery of carbon-nanotube-filled thermoplastic elastomers. Nature Mater 2004;3:115–8.
[60] Levitsky IA, Kanelos PT, Woodbury DS, Euler WB. Photoactuation from a carbon nanotube – Nafion bilayer composite. J Phys Chem B 2006;110:9421–5.
[61] Courty S, Mine J, Tajbakhsh AR, Terentjev EM. Nematic elastomers with aligned carbon nanotubes: new electromechanical actuators. Europhys Lett 2003;64:654–60.
[62] Ahir SV, Squires AM, Tajbakhsh AR, Terentjev EM. Infrared actuation in aligned polymer–nanotube composites. Phys Rev B 2006;73:085420.
[63] Ahir SV, Terentjev EM. Fast relaxation of carbon nanotubes in polymer composite actuators. Phys Rev Lett 2006;96:133902.
[64] Lu SX, Panchapakesan B. Photomechanical responses of carbon nanotube/polymer actuators. Nanotechnology 2007;18:305502.
[65] Huber JE, Fleck NA, Ashby MF. The selection of mechanical actuators based on performance indices. Proc Roy Soc Series A 1997;453:2185–205.
[66] Lynch M, Patrick D. Organizing carbon nanotubes with liquid crystals. Nano Lett 2002;97:1197–201.
[67] Dierking I, Scalia G, Morales P, LeClere D. Aligning and reorienting carbon nanotubes with nematic liquid crystals. Adv Mater 2004;16:865–9.
[68] Burylov SV, Raikher YL. Orientation of a solid particle embedded in a monodomain nematic liquid crystal. Phys Rev E 2004;50:358–67.
[69] Taya M, Kim WJ, Ono K. Piezoresistivity of a short fiber/elastomer matrix composite. Mech Mater 1998;28:53–9.
[70] Munson-McGee SH. Estimation of the critical concentration in an anisotropic percolation network. Phys Rev B 1991;43:3331–6.
[71] Zheng X, Forest MG, Vaia R, Arlen M, Zhou R. A strategy for dimensional percolation in sheared nanorod dispersions. Adv Mater 2007;19:4038–43.
[72] Koerner H, Liu WD, Alexander M, Mirau P, Dowty H, Vaia RA. Deformation-morphology correlations in electrically conductive carbon nanotube thermoplastic polyurethane nanocomposites. Polymer 2005;46:4405–20.
[73] Hon KK, Corbett D, Terentjev EM. Thermal diffusion and bending kinetics in nematic elastomer cantilever. Eur Phys J E 2008;25:83–9.
[74] Verissimo-Alves M, Capaz RB, Koiller B, Artacho E, Chacham H. Polarons in carbon nanotubes. Phys Rev Lett 2001;86:3372–5.
[75] Ajayan PM, Terrones M, de la Guardia A, Huc V, Grobert N, Wei BQ, et al. Nanotubes in a flash - Ignition and reconstruction. Science 2002;296:705.
[76] Lu SX, Ahir SV, Terentjev EM, Panchapakesan B. Alignment dependent mechanical responses of carbon nanotubes to light. Appl Phys Lett 2007;91:103106.
[77] Baughman RH, Cui CX, Zakhidov AA, Iqbal Z, Barisci JN, Spinks GM, et al. Carbon nanotube actuators. Science 1999;284:1340–4.
[78] Berhan L, Yi YB, Sastry AM, Munoz E, Selvidge M, Baughman RH. Mechanical properties of nanotube sheets: alterations in joint morphology and achievable moduli in manufacturable materials. J Appl Phys 2004;95:4335–45.
[79] Vohrer U, Kolaric I, Haque MH, Roth S, Detlaff-Weglikowska U. Carbon nanotube sheets for the use as artificial muscles. Carbon 2004;42:1159–64.
[80] Jaeger HM, Liu CH, Nagel SR. Relaxation at the angle of repose. Phys Rev Lett 1989;62:40–3.
[81] Clarke SM, Terentjev EM. Slow stress relaxation in randomly disordered nematic elastomers and gels. Phys Rev Lett 1998;81:4436–40.

Samit Ahir is a Group Executive for the Makevale Group where, amongst other roles, he currently oversees commercial nanocomposite research and development. He received MEng in Material Science from Imperial College London in 2003, and PhD in Experimental Physics from Cambridge University in 2006. He has worked in UK and USA, as well as founded a charity and dance company in 2005. He is a FreshMinds Ones to Watch™'s selected mind.

Yan Yan Huang received her MEng in Material Science from Imperial College London in 2007, and is currently a PhD candidate in Department of Physics (Cavendish Laboratory) in Cambridge. Her research interests include stabilization of carbon nanotubes in elastomeric matrices and dielectric properties of CNT–polymer composites, and their applications in material science and electronic engineering.

Eugene Terentjev is a Professor of Polymer Physics at University of Cambridge. He received his PhD in 1985 in Moscow for theoretical research in liquid crystals, and did postdoctoral work on modeling l.c. polymers in CWRU, Ohio. After moving to Cambridge University in 1992, he worked extensively on theory and experiment in liquid crystalline elastomers, and is a coauthor (with Mark Warner) of the monograph on this subject. He is interested in a wide range of problems in soft-matter and biological physics, developing theories and supervising the experimental laboratory researching structure, optical and mechanical properties, and rheology of complex materials.